JOURNAL OF OPTOELECTRONICS AND ADVANCED MATERIALS, Vol. 11, No. 11, November 2009, p. 1660 - 1670

Multispectroscopic investigation of silanised glass particles for dental fillers

S. SIMON*, R.V. F. TURCU, T. RADU, M. MOLDOVAN[a], V. SIMON
Babes - Bolyai University, Faculty of Physics, 400084 Cluj-Napoca, Romania
[a]Babes - Bolyai University, Raluca Ripan Institute of Chemistry, 400294 Cluj-Napoca, Romania

Aluminosilicate glasses containing similar aluminium oxide amount, considered as components of dental glass-ionomer cements are investigated. The paper aims a correlation between the surface structure of dental glass fillers and their bioactivity in simulated body fluid (SBF). Analyses carried out by Fourier Transform Infrared (FTIR), Magic Angle Spinning Nuclear Magnetic Resonance (MAS-NMR) and X-ray photoelectron spectroscopy (XPS) on samples before and after immersion in SBF show differences regarding both structural units and bioactivity, function of silanisation degree. The investigation methods used in this study complementary contribute to highlight the changes of the local structure on the surface interacting with SBF. The results show that using gamma-methacryloxypropyl trimethoxysilane the less silanised glass filler is more bioactive than the highly silanised ones.

(Received September 24, 2009; accepted November 12, 2009)

Keywords: Glass ionomer, Silanisation; Bioactivity, MAS-NMR, FTIR, XPS

1. Introduction

Dental materials in restorations are essentially oxide based glass and glass-ceramic systems. Glass ionomer cements, first developed and reported by Wilson and Kent [1], are dental restoration materials that bond chemically to tooth hard tissues and release fluoride for a relatively long period. They are composed of glass powder and a

polycarboxylic acid. The most utilised glasses are calcium aluminosilicate glasses containing some fluoride. Glass ionomer cements can be expected to own characteristics of both the silicateglasses, i.e. translucency and fluoride release, and of the polycarboxylates, i.e. ability to chemically bond to tooth structure and agreeableness for the pulp [2]. The powder phase of a glass ionomer consists of an ion-leachable calcium alumino-fluoro-silicate glass system.

Bioactive glasses are surface-active bone substitutes that have shown good biocompatibility both with bone and with soft tissue and are used in oral and maxillofacial bone augmentation [3]. Developments are directed towards the production of material with a suitable surface which will become invaded by bone or by connective tissue.

In the last decades, glass-ionomer cements have attracted increasing interest in the area of dental materials [4-7]. Their major advantage consists in the ability to adhere permanently to the hydrophilic surfaces of hard oral tissues, thus offering the possibility of sealing margins developed at the tissue interfaces during restorative procedures [8].

This study is mainly focussed on the structural changes occurred in the local order of several aluminosilicate glass systems usable as filler in dental implant cements, and their in vitro bioactivity.

2. Materials & methods

The composition of the investigated aluminosilicate systems is given in Table 1. Fluorides were added to the oxide components in order to diminish the melts viscosity and implicitly the melting temperature [9], and at the same time to ensure a long term fluoride release, due to the fact that a proper amount of fluoride helps to prevent and control dental caries [10].

Table 1. Sample composition in wt %.

Sample code	Components (wt %)							
	SiO_2	Al_2O_3	B_2O_3	BaO	ZnO	SrO	ZrO_2	fluorides
S1	45	10	17	20				8
S2	40	10	10		30			10
S3	40	10	5			27	8	10

The samples were prepared by quickly undercooling to room temperature from melting temperatures comprised between 1300 and 1400°C, depending on glass composition. The micrometric sized particles of finely ground samples were treated with silane A-174 (gamma-methacryloxypropyl trimethoxysilane), because silane is a coupling agent that bonds the glass particles to the polymer matrix. During fabrication of filler composites, the silanisation process is a critical step [11], upon which depend the physical properties of glass ionomer cements and their resistance to hydrolytic degradation [12]. In order to have a first test on bioactivity of the glass fillers, they were exposed to simulated body fluid (SBF) for seven days at 37°C. The SBF was prepared according to Kokubo protocol [13], one of the most frequently used solution

simulating the body fluid, because it contains inorganic ions in concentrations very close to those of human blood plasma.

The FTIR spectra were recorded on a Bruker spectrometer at room temperature in the wavenumbers range from 400 to 4000 cm^{-1}, using the KBr disk technique. The ^{31}Si (I=1/2), ^{27}Al (I=5/2), ^{11}B (I=3/2) and ^{31}P (I=1/2) MAS NMR spectra were recorded at room temperature from powder samples on MAS NMR AVANCE 400 Bruker spectrometer, in magnetic field of 9.4 T, at 79.5, 104.2, 128.4 and 161.9 MHz, and spinning frequency of 8, 15, 10 and 9 kHz, respectively. References for the chemical shift (0 ppm) were tetramethylsilane (TMS) for ^{29}Si, 1 M aqueous $Al(NO_3)_3$ solution for ^{27}Al, 1 M aqueous H_3BO_3 solution for ^{11}B, and 85 % H_3PO_4 water solution for ^{31}P. The experimental spectra were simulated using the DMfit program [14]. X-ray Photoelectron Spectroscopy (XPS) analyses were performed on SPECS PHOIBOS 150 MCD system with monochromatised Al-K_α radiation from a 300 W X-ray source (hν=1486.6 eV). The measurements were performed under ultra high vacuum conditions, of order 10^{-10} Torr. The binding energy scale was calibrated using the C 1s line at 284.6 eV.

3. Results and discussion

X-ray powder diffraction patterns (Fig. 1) of the samples prepared by quickly undercooling of melts consist of broad lines typical of glass systems. The silane adherence on surface of the powdered samples is confirmed by both FTIR and XPS results. The occurrence of the IR absorption bands around 1720 cm^{-1} is assigned to carbonyl (–C = O) group of silane [15].

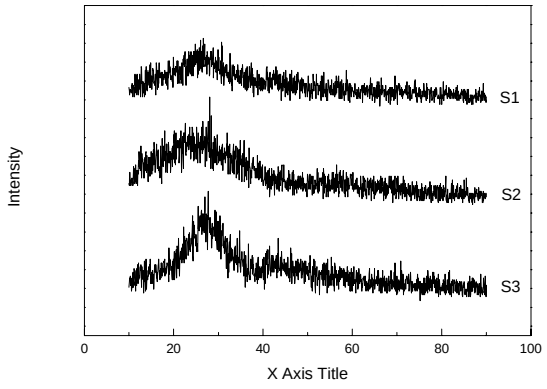

Fig. 1. X-ray diffraction pattern of glass fillers

As can be seen in Fig. 2, this band is better developed in the case of S1 and S2 samples, indicating that for these glasses the silanisation process was more efficient, and is much weaker for the sample S3.

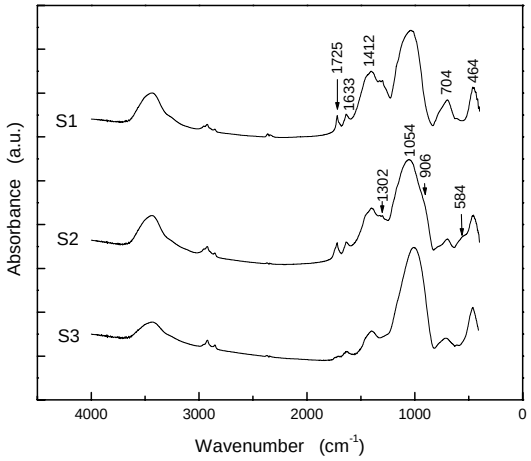

Fig. 2. FTIR spectra of silane treated samples

Additional information on carbon bonds and implicitly on glass filler silanisation provide the high-resolution C 1s XPS scans (Fig. 3). In order to extract quantitative information on silane attachment on glass particles, the contribution of the components arising around 285, 286 and 288 eV from C-C/C-H, C-O and C=O, respectively, was calculated using the fitting of C 1s photoelectron peak. The contributions of carbons implied in C-O and C=O bonds, which can be ascribed only to silane in the investigated samples, is 20 % for S1, 37 % for S2 and 8.7 % for S3 glass particles.

In terms of further analysis of FTIR spectra (Fig. 2), the large absorption band at 3450 cm^{-1} and the weak narrow band at 1633 cm-1 are related to O–H stretching of water molecules [16]. The intense IR band recorded around 1050 cm^{-1} is assigned to the asymmetric stretching vibration of Si-O-Si bonds between SiO_4 tetrahedra [17, 18]. The Si–O–Si bend vibrations lead to the IR absorption peak around 460 cm^{-1} [19]. In fact, in the spectral region from 900 to 1100 cm^{-1} are expected IR absorption bands from differently connected SiO_4 tetrahedra, from double silicon tetrahedra linked by one bridging oxygen (Si_2O_7 units at 900 cm^{-1}), to silicon tetrahedra with all four bridging oxygens implied exclusively in Si-O-Si linkages (1100 cm^{-1}) like in pure SiO_2 [20]. The contribution of these units could be evaluated by decomposition of IR absorption bands in this region, using components centred at wavenumbers predicted from second derivative of the spectra. The complex composition of the investigated glasses limits the accuracy of such a prediction due to the shifts occurred from several components.

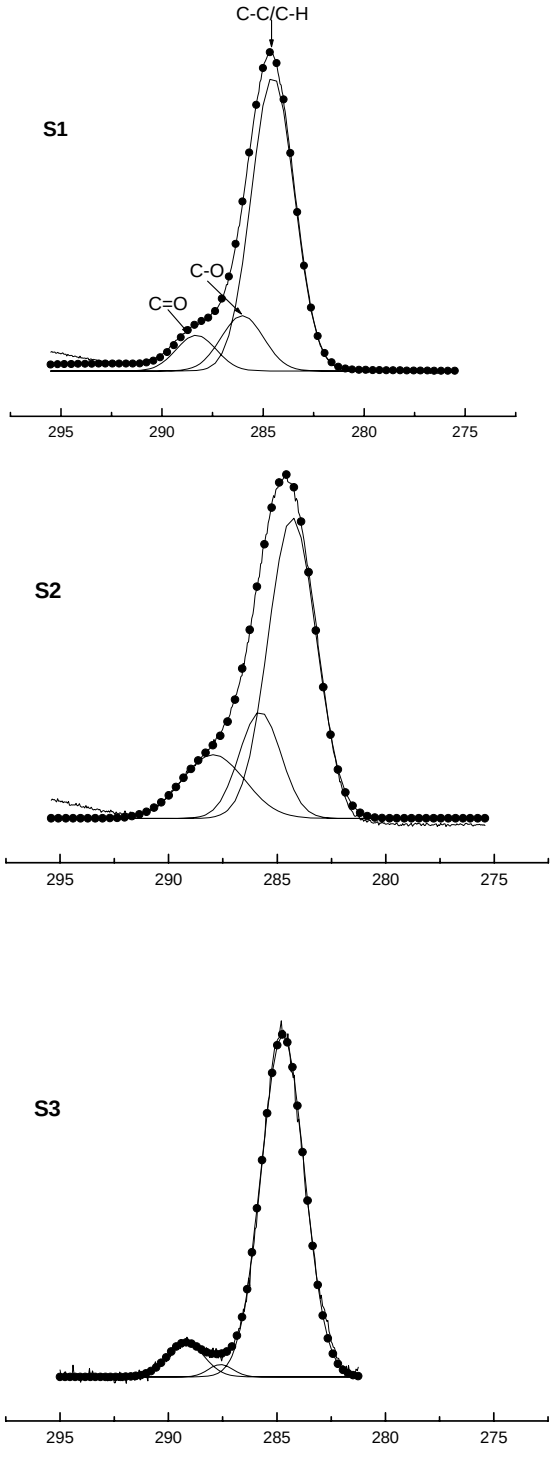

Fig. 3. C 1s core level XPS spectra of silane treated samples

With respect to aluminium local structure, the FTIR spectra have to be inspected in the region below 900 cm^{-1}, wherein the contributions from the aluminium polyhedra are recorded. For example, in zeolitic alkali aluminosilicates [21] the occurrence of an IR absorption band around 550 cm^{-1} was assigned to octahedral Al coordination, Al_{VI} (in AlO_6 units) and around 800 cm^{-1} to tetrahedral Al coordination, Al_{IV} (in AlO_4 units). Between these two relatively large regions would appear bands corresponding to penta-coordinated aluminium atoms, if there are [22]. The spectra of our samples show stretching vibrations at 704 cm^{-1} related to aluminium and oxygen atoms from AlO_4 structural units, typical for the Al-O bonds in these tetrahedra [23]. The IR absorption bands for the stretching modes of AlO_6 structural units occur in 650 – 400 cm^{-1} region [23], but around 460 cm^{-1}, in aluminosilicate samples, the Si–O–Si bend vibrations gives also rise to an IR absorption [19]. Due to this superposition of the absorption bands, it is not possible for these samples to appreciate quantitatively the relative coordination of aluminium in AlO_4 and AlO_6 structural units from IR data.

The peaks around 1400 cm^{-1} arise from tricoordinated boron, B_{III} (in BO_3 units). For S1 and S2, there are two infrared-active peaks at 1412 and 1302 cm^{-1} ascribed to asymmetric trigonal B-O stretching. One observes that the intensity of this IR absorption line decreases in the series S1, S2, S3, that can be related at first glance to the decreasing B_2O_3 content in these samples. For S2 the large 1054 cm-1 absorption band is broadened by a shoulder at 906 cm-1. In borate glasses the tetracoordinated boron atoms, B_{IV} (in BO_4 units), lead to IR absorption bands in the region between 800 and 1100 cm^{-1}, and the B–O–B bending vibrations manifest in the lower frequency region between 600 and 800 cm^{-1} [24-27]. In fact, in 600–1000 cm^{-1} region, it is very difficult to assign the IR bands, because to this spectral range can contribute absorptions related to both symmetric and asymmetric tetrahedral B-O stretching, as well as symmetric trigonal B-O stretching and peaks due to B-O-H bending [27]. At the same time, as mentioned above, in the same spectral ranges occur also IR absorption bands from silicate and aluminate units.

The FTIR spectra recorded from glass fillers immersed for seven days in simulated body fluid do not evidence changes in position and relative intensity of the absorption bands before immersion in SBF. Only a very slight broadening of the absorption bands was observed, that may be associated with a randomisation of the structural units on samples surface. Calcium phosphate groups were expected to be formed on glass filler surface after immersion in SBF, but the IR characteristic peaks of phosphate groups, if there are, could not be certainly evidenced because they appear between 1090-1030 and 600-560 cm^{-1} [28], where are recorded the prevalent IR absorption bands from silicate and aluminate units. The limitations presented above in identifying from IR analysis the structural units of the investigated glass fillers can be overpassed to a great extent by the results obtained from ^{29}Si, ^{27}Al and ^{11}B nuclear magnetic resonance analysis. Despite these difficulties, the IR results bring useful information for the discussion of NMR data.

Solid-state magic angle spinning nuclear magnetic resonance (MAS-NMR) spectroscopy has been previously used for investigation of glass ionomer cements [5-7, 29].

Fig. 4 shows the ^{29}Si MAS-NMR spectra of the investigated samples. A large peak with chemical shift in the range from -94 to -99 ppm dominates the spectrum of each sample. The chemical shift indicates the environment around the Si atoms in the glasses. Considering the four coordinated state of silicon in SiO_4 tetrahedra linked to form the silicate glass network, according to $Q^{(n)}$ notation, where $n \leq 4$ represents the number of bridging oxygen, the values of the chemical shifts denote the presence of certain silicate units/species [30].

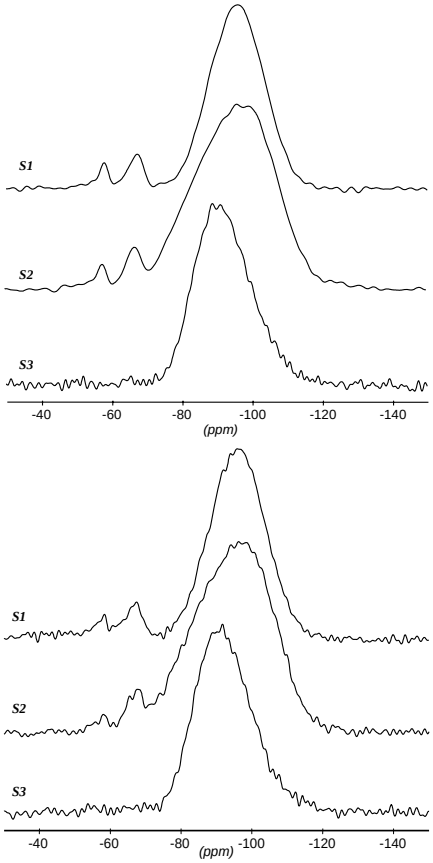

Fig. 4. ^{29}Si MAS NMR experimental spectra before (a) and after SBF immersion (b).

Each $Q^{(n)}$ species is equivalent to an anion with a negative charge of -(4-*n*), which is balanced by the positive charge of a modifier cation [30]. The distribution of silicate tetrahedra, commonly described as $Q^{(n)}$ species, is the most important aspect of this speciation, and can be estimated from ^{29}Si MAS- NMR spectra by deconvolution with components having chemical shifts corresponding to different $Q^{(n)}$ units. The chemical shift depends on the number of bridging oxygens (BO) and nonbridging oxygens (NBO) attached to silicon atoms. The ^{29}Si chemical shift is more negative as the number of bridging oxygen linkages increases, due to a greater degree of electronic shielding of the silicon atom. Increasing of NBO number moves the peak to smaller values of chemical shift [6], and this is the case easily visible from Fig. 4a for S3 sample.

A circumspect assignment of the components obtained by ^{29}Si MAS- NMR spectra deconvolution (Fig. 5) was considered with respect to $Q^{(n)}$ units. The first approach was to identity $Q^{(n)}$ species according to corresponding values of chemical shifts. Five kinds of $Q^{(n)}$ species seems to be present in S1 and S2 glasses, and only three in S3 glass.

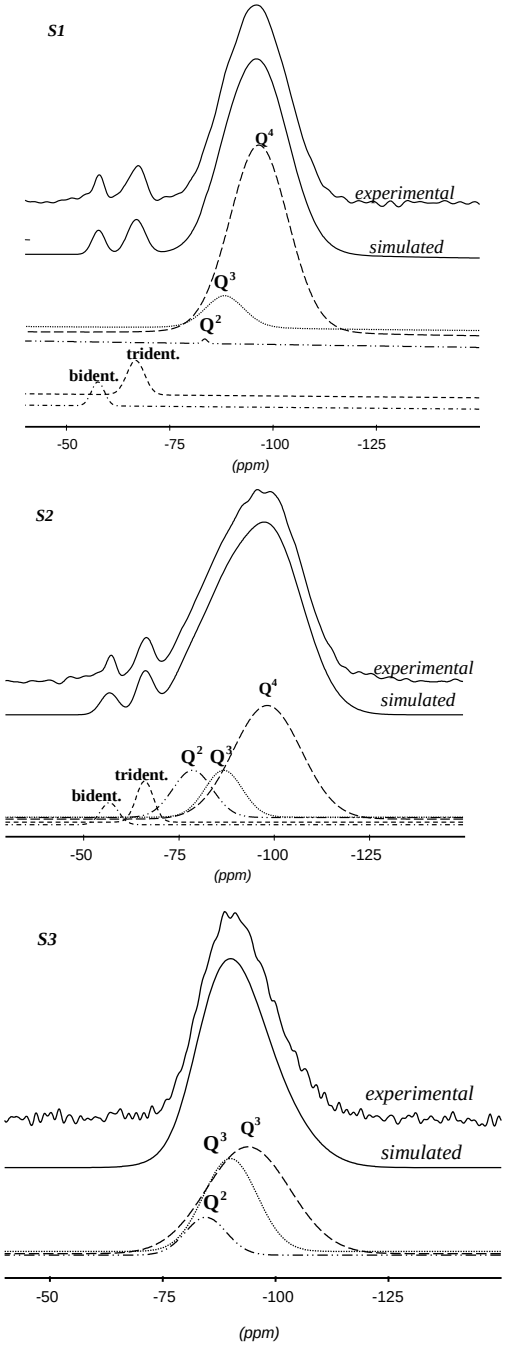

Fig. 5. ^{29}Si MAS NMR experimental and simulated spectra along with the deconvolution components, for S1 sample.

By taking into account that the weakest silanisation was observed in FTIR spectra for S3 sample, it appears plausible to reflect on occurrence of the two additional peaks in S1 and S2 spectra on the account of silanisation process, because it was reported [31] that monodentate, bidentate and tridentate attachment forms of silane on silica gel surface lead to ^{29}Si MAS-NMR signals at −48.5,−56.9 and −66.3 ppm, respectively. In our samples only peaks at around -66 and -57 ppm reflecting that in these samples only bidentate and tridentate forms are According to the results obtained for boro-alumosilicate glasses [32], the values of ^{29}Si chemical shift in the range from -88 to -101 ppm ascribed to Si-atoms in $Q^{(3)}$ units, with three bridging oxygens sharing SiO_4 tetrahedra and one non-bridging oxygen, can be also considered for Si-atoms of $Q^{(4)}$ units in which one or even two of the four bridging oxygens is in a Si–O–Al linkage. It is not excluded the possibility that the next nearest neighbour cations of $Q^{(4)}$ units are not silicon, but other network formers like aluminium or boron, that slightly moves the chemical shift of ^{3i}Si in $Q^{(4)}$ units to less negative values. We adopt this approach and assume that in the investigated glass fillers the most part of silicon atoms are implied in $Q^{(4)}$ units sharing part of their bridging oxygens with aluminium or boron tetrahedra. This assumption is supported by the high values for binding energy of O 1s photoelectrons, about 532 eV, that indicates the undoubted preponderance of bridging oxygens in these glasses (Fig. 6). The number of nonbridging oxygens, related to the deconvolution component at 530 eV, decreases from 8% in S1 to 18% in S2, and 22% in S3.

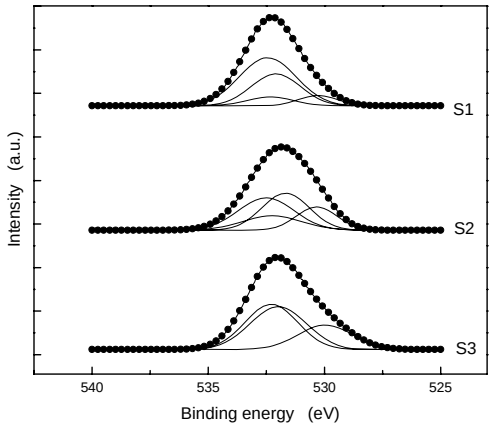

Fig. 6. O 1s core level XPS spectra of silane treated samples

Therefore, it appears more appropriate to assign the -95 ppm component to Q^4 species which are not exclusively bridged with SiO_4, but also with AlO_4 and possible with BO_4 units.

Taking into account the population of $Q^{(n)}$ species (Table 2) and the participation to each of them of bridging and nonbridging oxygens, the expected percentage of bridging oxygens for glasses S1, S2 and S3 is 85, 80 and 77 %, respectively, that shows a satisfactory agreement with the values estimated from O 1s core level XPS spectra.

Table 2. The distribution of silicate tetrahedra, $Q^{(n)}$, isotropic chemical shift, δiso, full width at half maximum, FWHM, of corresponding component lines, and the distribution of $Q^{(n)}$ units expressed by the relative intensity, I.

Sample	$Q^{(n)}$	δ_{iso} *(ppm)*	FWHM *(ppm)*	I *(%)*
S1	$Q^{(4)}$	-95.9	16.7	83.3
	$Q^{(3)}$	-88.1	11.2	10.0
	$Q^{(2)}$	-84.2	1.5	0.1
	silane trident.	-66.9	5.0	4.4
	silane bident.	-57.7	3.7	2.2
S2	$Q^{(4)}$	-98.7	21.0	73.3
	$Q^{(3)}$	-87.2	11.5	9.9
	$Q^{(2)}$	-79.1	12.2	10.6
	silane trident.	-66.6	5.3	4.0
	silane bident.	-57.3	5.5	2.2
S3	$Q^{(4)}$	-94.1	21.8	57.7
	$Q^{(3)}$	-90.1	14.0	32.3
	$Q^{(2)}$	-84.7	10.7	10.0

According to these data, a higher NBO number is evidenced with diminishing of SiO_2 content in S1-S3 glasses, and for the same SiO_2 content in S2 and S3 samples the increase of NBO number in S3 sample is due to the glass modifier role played by SrO in the silicate network, and similarly acts ZnO in S2 sample, but the effect of SrO is more pronounced because the cationic field strength, expressed by the ratio of the cation charge to the square of the ionic radius, of strontium is more than three times lower than that of zinc, namely 1.15 Å^{-2} for Sr^{2+} and 3.65 Å^{-2} for Zn^{2+} ions [33].

The NMR parameters and $Q^{(n)}$ species distribution determined from 29Si MAS NMR spectra are given in Table 2. The relative population for each of the identified $Q^{(n)}$ species indicates that $Q^{(4)}$ species dominates in all glasses. The next population is that of $Q^{(3)}$ species. Instead of $Q^{(0)}$ and $Q^{(1)}$ species we consider that the resonance peaks recorded at -57 and -66 ppm are related to silane attached on glass powder surface. The contribution of these components both for S1 and S2 glasses is about 6.5 %.

In contrast to crystalline silicates for which the isotropic line widths are usually narrow, on the order of 1 ppm or less, in silicate glasses the isotropic line widths are inhomogeneously broadened to over 10 ppm due to a continuous distribution of isotropic chemical shifts, which arise from a continuous structural distribution in local structure [34]. The full width at half maximum points onto the chemical shift distribution and at the same time onto the disorder in the glass network. For the width of $Q^{(n)}$ peaks (Table 2), is noticed a broadening with SiO_2 content diminishing. It is worth to mention that the weakest silanisation in FTIR spectra was observed for S3 sample, and, on the other hand, the ^{29}Si MAS NMR spectrum shows for the same sample the largest FWHM and the largest chemical shift of the prevalent $Q^{(4)}$ species to more positive values, suggesting the increase of NBO number.

Al_2O_3 belongs to intermediate oxides which can play both former and modifier role in the glass network. In aluminosilicate glasses is discussed on the Al avoidance defined using the relative lattice energy differences among the linkages Si-O-Si, Si-O-Al, and Al-O-Al [34]. For Si/Al ratio equal to 1 is realised the strict aluminium avoidance that makes Al-O-Si linkage more favourable than the

combination of Si-O-Si and Al-O Al, and the aluminosilicate glass structure is realised by AlO_4 tetrahedra connected only with SiO_4 tetrahedra [34].

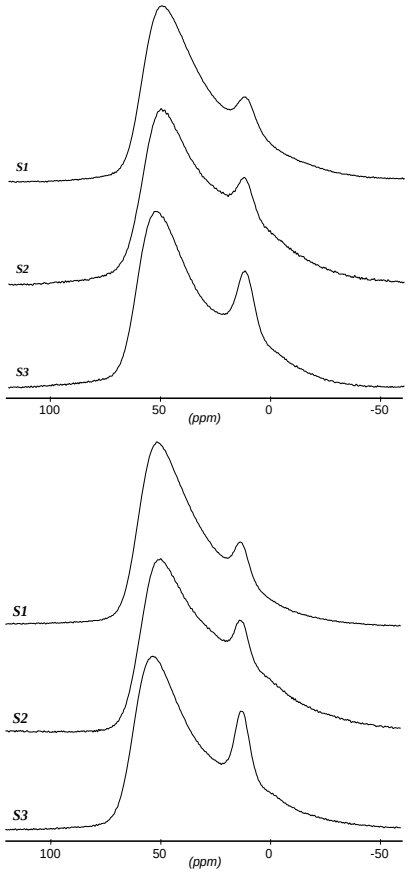

Fig. 7. ^{27}Al MAS NMR experimental spectra before (a) and after SBF immersion (b).

In an aluminosilicate glass network is considered that the structural unit can be expressed as $Q^n(mAl)$, $Si(OSi)_{n-m}(OAl^-)_m(O^-)_{4-n}$, where n is the number of bridging oxygens bonded to the Si tetrahedron, $0 \le n \le 4$, and m is the number of Al atoms as a second nearest neighbours, $m \le 4-n$, and the ^{29}Si chemical shift increases with decreasing n or increasing m [6, 29, 35]. The shift depends on the number of bridging and nonbridging oxygens attached to the silicon. Increasing the number of NBO moves the peak to more positive values, whilst increasing the number of next nearest neighbour aluminium atoms moves the peak to more negative values. Due to the different components entering in these samples beside SiO_2 and $Al2O_3$, it is difficult to have a univocal explanation based only on aluminosilicate structural units. For S3 glass the increase of NBO number is primary caused by the addition of SrO glass network modifier, without to exclude that also and ZrO_2 acts also as modifier, even though the cationic field strength of zirconium is quite high, 6.25 Å^{-2}. The results obtained support that in these glass fillers the prevalent aluminosilicate structural unit is of $Q^4(1Al)$ type [6, 29].

NMR investigation of ^{27}Al nuclei inform more properly on aluminium surrounding in aluminosilicate systems. Fig. 7 shows the ^{27}Al MAS NMR spectra recorded from the investigated glasses. The isotropic chemical shifts are extended from 53 ppm to 9 ppm. Usually, the ^{27}Al MAS NMR spectra in amorphous and crystalline aluminates [36-43] consist of three lines centred at 0-10 ppm, 20-40 ppm and 50-70 ppm corresponding to three types of aluminium: hexa- penta- and tetra-coordinated with ogygens, respectively [44, 45]. In the case of our samples the spectra show that the contributions are coming only from tetra- and hexa-coordinated aluminium (Fig. 8).

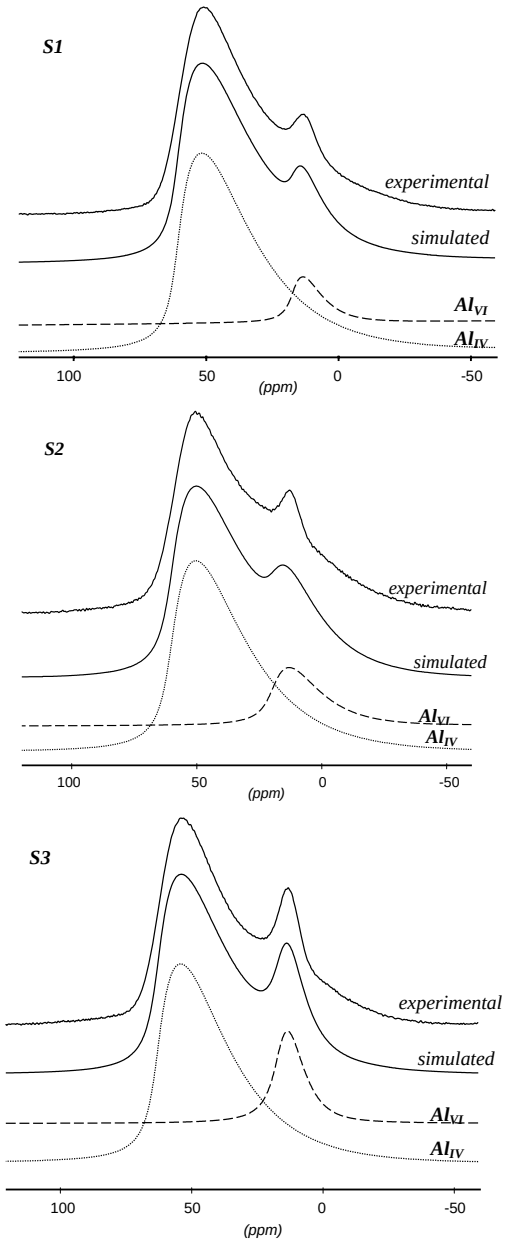

Fig. 8. ^{27}Al MAS NMR spectra with it deconvolution

In order to estimate the relative number of tetracoordinated to hexacoordinated aluminium atoms we considered the ratio between the analytical integration accounts of the two corresponding peaks of the NMR

spectra. The values obtained are summarised in Table 3 The AlO_4 structural units are prevalent versus AlO_6 ones. The relative contribution of Al^{IV} decreases with the Si/Al ratio of the glasses studied. This behaviour is in agreement with data reported for sodium aluminosilicate glasses [46].

Table 3. ^{27}Al NMR parameters and aluminium sites distribution expressed by the relative intensity, I. δiso is the isotropic chemical shift, C_Q is the quadrupole coupling constant and η_Q is the quadrupolar asymmetry parameter.

Sample	Al_{IV}				Al_{VI}			
	δ_{iso} *(ppm)*	C_Q *(kHz)*	η_Q	I *(%)*	δ_{iso} *ppm)*	C_Q *(kHz)*	η_Q	I *(%)*
S_1	50.2	5620	0.1	90.9	12.3	3103	0.9	9.1
S_2	50.3	5682	0.1	82.6	13.5	4177	0.9	17.4
S_3	53.2	5404	0.1	82.4	12.7	2459	0.9	17.6

The quadrupolar coupling constants C_Q are consistent with the values reported for commercial glass ionomer cements [5, 7]. Based on the composition of the glasses, the most probable next nearest neighbours of aluminium are the silicon atoms.

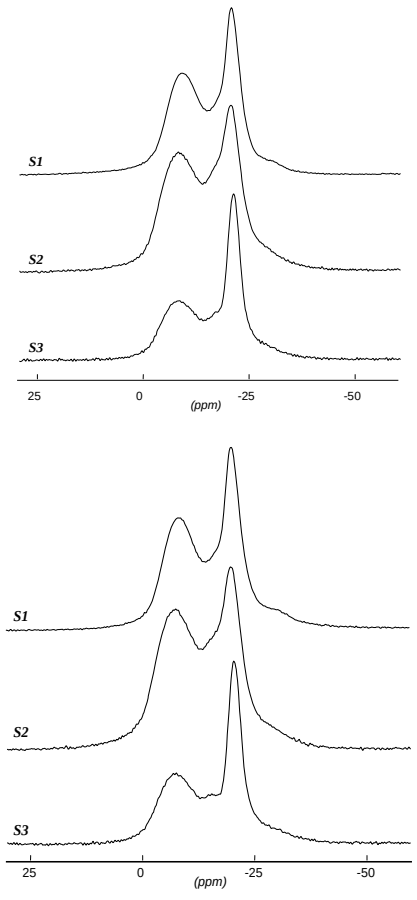

Fig. 9. ^{11}B MAS NMR experimental spectra before (a) and after SBF immersion (b).

The tetracoordinated aluminium represents the usual structural units in aluminosilicates [9]. The fluoride addition to aluminosilicate glass systems promotes the occurrence of hexacoordinated aluminium species [44]. In our samples the amount of hexacoordinated aluminium is higher in S2 and S3 glasses, with less SiO_2 content, and it is likely that in S3 sample, the addition of SrO glass network modifier also contribute to an octahedral environment of aluminium. The increase of hexa-coordinated aluminum could also denote a phase separation and increased tendency for crystallisation [6], i.e. a diminished glass stability. It is worth noticing that no peak suggesting the presence of pentacoordinated aluminum is present in these glasses. Comparing our NMR data with those reported for ionomer commercial glasses, one remarks a very good agreement with respect to Al_{IV} population [6,7].

The glass network former B_2O_3 delivers two boron sites. In pure B_2O_3 glass the large majority of BO_3 basic structural units are connected in boroxol rings, while other units form together new BO_4 units, more stable than BO_3 [47].

^{11}B MAS NMR spectra collected from the three glasses containing boron are shown in Fig. 9. The spectra indicate the presence of both B_{III} (in BO_3 unit) and B_{IV} (in BO_4 unit) species. The sharp peak about –20 ppm is attributed to BO_4 tetrahedra, and the broad peak about –7 ppm is assigned to trigonal BO_3 units [45, 48]. The contribution of BO_3 and BO_4 groups was evaluated based on the deconvolution of the spectra (Fig. 10). The peak areas were analysed and B_{IV}/B_{III} ratio was calculated (Table 4). Despite the low B_2O_3 content in these glasses, boron preponderantly occurs in BO_3 structural units. The quadrupolar coupling constant for tetra-coordinated boron atoms in much lower, <1 MHz, than for the three-coordinate ones, 2.4 – 2.9 MHz [49] and this is useful to distinguish between the population of the two boron species. A narrow resonance is expected from BO_4 units with lower C_Q values and a broad resonance is expected for BO_3 units, which have much larger C_Q values.

Table 4. ^{11}B NMR parameters (δ_{iso} - isotropic chemical shift, C_Q - quadrupole coupling constant, η_Q - quadrupolar asymmetry parameter) and boron sites distribution expressed by the relative intensity, I.

Sample	B_{III}				B_{IV}			
	δ_{iso} *(ppm)*	C_Q *(kHz)*	η_Q	I *(%)*	δ_{iso} *ppm)*	C_Q *(kHz)*	η_Q	I *(%)*
S_1	-7.9	1636	0.2	59.4	-20.1	576	0.8	40.6
S_2	-7.3	2009	0.2	66.9	-19.7	598	0.8	33.1
S_3	-7.5	2106	0.2	56.0	-20.4	596	0.8	44.0

As already mentioned, the numerous components of the investigated glass fillers make difficult a univocal/ unambiguous discussion on the B_{III} and B_{IV} populations in these samples. An aspect, that seems to be in this point in disagreement with the IR results, is related to IR

absorption bands centred around 1412 cm^{-1}, assigned to BO_3 units. According to intensity of this IR band, and corresponding to composition of the samples, the number of BO_3 units evidently decreases in S1-S2-S3 series, that is by far not the result obtained from ^{11}B MAS NMR analysis. On the other hand the IR absorption band about 1412 cm^{-1} is not the sole IR absorption that can arise from BO3 units, but the other are in the same spectral region where are occurring the absorption bands from the preponderant silicon species. Nevertheless, another reason could consist in the inaccuracy of ^{11}B MAS NMR data obtained in the low 9.4 T field, with respect to B_{III} and B_{IV} populations.

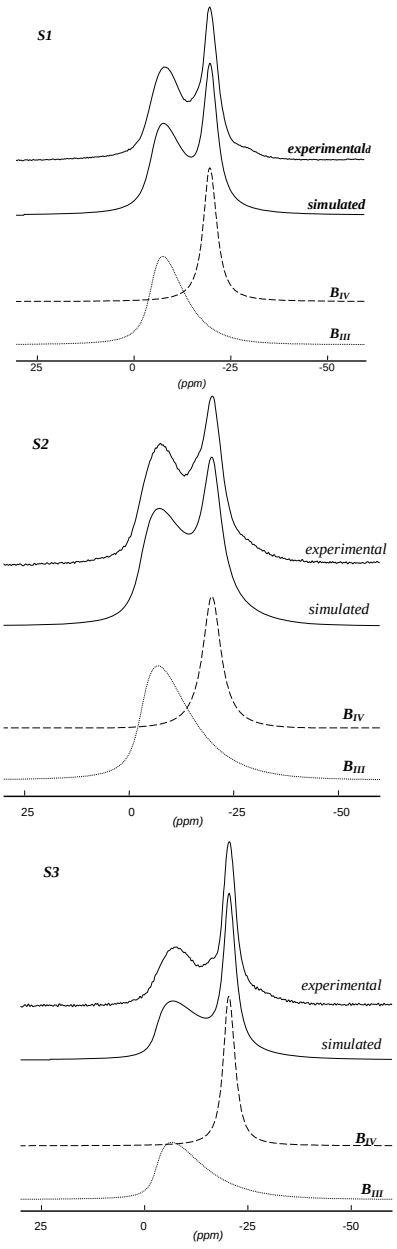

Fig. 10. ^{11}B MAS NMR spectra with it deconvolution

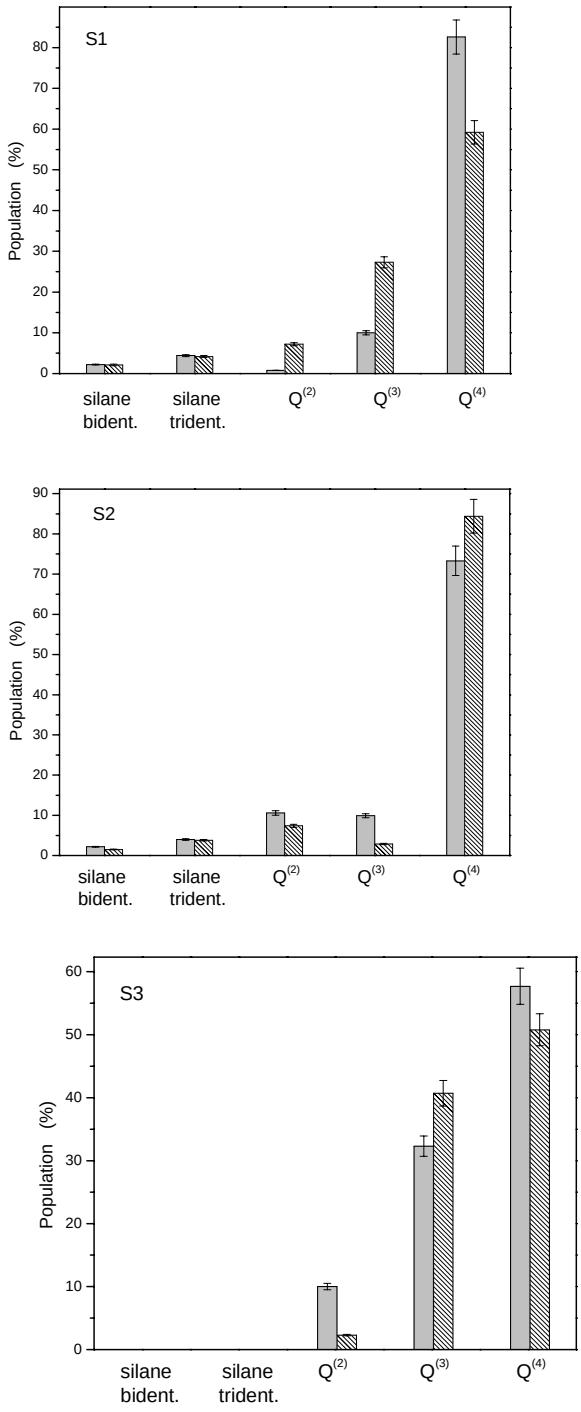

Fig. 11. Distribution of $Q^{(n)}$ species before (grey columns) and after SBF immersion (striped columns).

After seven days immersion of glass fillers in simulated body fluid (SBF), sensible changes are observed in the NMR spectra (Figs. 4b, 7b and 9b). The results obtained by spectra analysis are shown in Tables 5-7.

Table 5. The $Q^{(n)}$ species distribution (I) from ^{29}Si MAS NMR experiments carried out after seven days immersion in SBF, isotropic chemical shift, δ_{iso}, full width at half maximum, FWHM.

Sample	$Q^{(n)}$	δ_{iso} *(ppm)*	FWHM *(ppm)*	I *(%)*
S1	Q^4	-99.16	14.73	59.2
	Q^3	-92.02	11.62	27.3
	Q^2	-84.96	9.59	7.2
	silane trident.	-67.01	4.75	4.2
	silane bident.	-57.85	10.43	2.1
S2	Q^4	-98.14	23.40	84.4
	Q^3	-86.49	7.86	2.9
	Q^2	-79.51	11.45	7.4
	silane trident.	-66.80	5.72	3.8
	silane bident.	-57.11	6.15	1.5
S3	Q^4	-95.24	22.03	50.9
	Q^3	-90.31	14.39	40.8
	Q^2	-84.06	6.69	2.4

Table 6. ^{27}Al NMR parameters and aluminium sites distribution expressed by the relative intensity, I. δiso is the isotropic chemical shift, C_Q is the quadrupole coupling constant and η_Q is the quadrupolar asymmetry parameter (spectra recorded from samples immersed for seven days in SBF).

Sample	Al_{IV}				Al_{VI}			
	δ_{iso} *(ppm)*	C_Q *(kHz)*	η_Q	I *(%)*	δ_{iso} *ppm)*	C_Q *(kHz)*	η_Q	I *(%)*
S1	50.1	5755	0.1	93.0	12.5	2200	0.9	7.0
S2	49.4	5747	0.1	92.7	13.3	4201	0.9	7.3
S3	52.8	5687	0.1	85.4	12.4	2753	0.9	14.6

Table 7. ^{11}B NMR parameters (δ_{iso} - isotropic chemical shift, C_Q - quadrupole coupling constant, η_Q - quadrupolar asymmetry parameter) and boron sites distribution expressed by the relative intensity, I. (Spectra recorded from samples immersed for seven days in SBF).

Sample	B_{III}				B_{IV}			
	δ_{iso} *(ppm)*	C_Q *(kHz)*	η_Q	I *(%)*	δ_{iso} *(ppm)*	C_Q *(kHz)*	η_Q	I *(%)*
S1	-7.7	1695	0.2	60.0	-20.3	580	0.8	40.0
S2	-7.5	2010	0.2	66.5	-20.0	600	0.8	33.5
S3	-7.4	2096	0.2	56.4	-20.5	592	0.8	43.6

As can be seen from Fig. 11 , for S1 sample the number of $Q^{(4)}$ species decreases, but that of $Q^{(2)}$ and $Q^{(3)}$ species increases, for S2 sample is noticed an increase of $Q^{(4)}$ species and decrease of $Q^{(2)}$ and $Q^{(3)}$, while for S3 sample increases the number of $Q^{(3)}$ species and that of $Q^{(2)}$ and $Q^{(4)}$ decrease. The changes regarding the presence of bidentate and tridentate attachment forms of silane on the surface of these samples are insignificant. Based on these data, an evaluation concerning the bioactivity and the population of different $Q^{(n)}$ species before and after immersion in SBF appears of low confidence.

The analysis of ^{27}Al MAS NMR spectra recoded from glass samples immersed for seven days in SBF points out (Table 6) a sensible higher population of tetracoordinated aluminium than before SBF immersion, relative to hexacoordinated aluminium, while the ^{11}B MAS NMR spectra do not evidence a change related to three- and tetracoordinated boron species (Table 7). Studies on silanised apatite-wollastonite glass ceramic [50] and 45S5 Bioglass®-based glass-ceramic scaffolds [51] tested in SBF showed that their bioactivity depends on silane treatment. The results obtained in our study show a higher bioactivity for the less silanised glass sample.

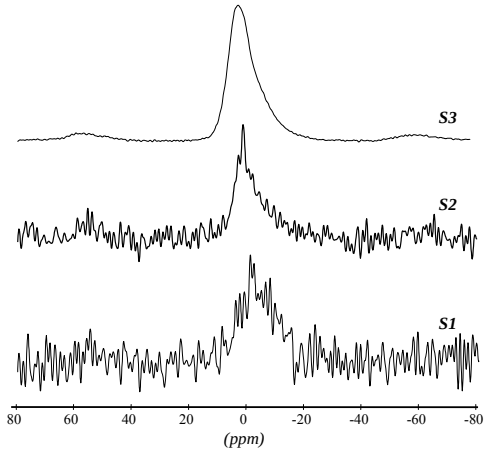

Fig. 12. ^{31}P MAS NMR spectra after SBF immersion.

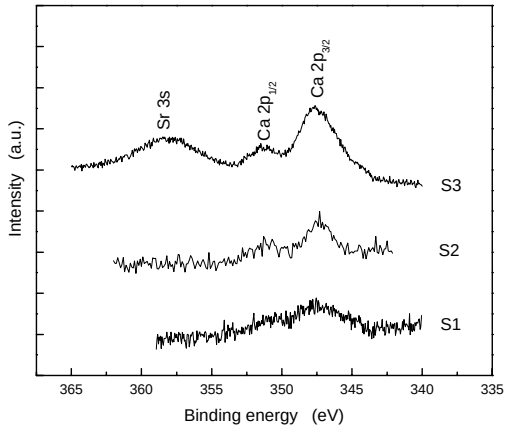

Fig. 13. Ca 2p core level XPS spectra.

Due to the expected selfassembling of a calcium phosphate layer on glass fillers soaked in SBF, ^{31}P MAS NMR spectra were recorded from all samples immersed in SBF (Fig. 12). At the same time, by means of XPS

analysis was evidenced the presence of calcium on these samples after SBF immersion (Fig. 13), that indicates the selfassemblation of calcium phosphates on samples surface. The growth of calcium phosphate coatings on glass filler surface upon immersion in SBF is an indication of the bioactivity of a material [13]. The core level spectrum of Ca 2p photoelectrons recorded from S3 glass sample supports again that this sample is more bioactive than S1 and S2 samples.

4. Conclusions

The local structure in the investigated dental filler materials depend on glass composition. $Q^{(4)}$ silicate tetrahedra are preponderent and the structural units of aluminosilicate glass network are of Q^4(1Al) type. Both tetra- and hexacoordinated aluminium atoms are evidenced, but neither IR nor NMR results indicate pentacoordinated aluminium. The silanisation treatment is less efficient for the sample containing glass network modifier oxides with low cationic field strength. A correlation between the bioactivity tested in simulated body fluid and the population of different $Q^{(n)}$ species appears of low confidence. In case of gamma-methacryloxypropyl trimethoxysilane, the bioactivity of the less silanised glass is higher than that of highly silanised glass samples.

References

[1] A. D. Wilson, B. E. Kent, Br. Dent. J., **132**, 133 (1972).
[2] D. G. Charlton, D. F. Murchison, B. K. Moore, J. Dent. **19**, 249 (1991).
[3] I. D. Xynos, A. I. Edgar, L. D. K. Buttery, L. L. Hench, J. M. Polak, J. Biomed. Mater. Res. **55**, 151 (2001).
[4] Y. Finer, J. P. Santerre, J. Biomed. Mater. Res. A, **81**, 75 (2007).
[5] R. Pires, T. G. Nunes, I . Abrahams, G. E. Hawkes, C. M. Morais, C. Fernandez, J. Mater. Sci.: Mater. Med. **15**, 201 (2004).
[6] A. Stamboulis, R. V. Law, R. G. Hill, Biomaterials **25**, 3907 (2004).
[7] R. A. Pires, T. G. Nunes, I. Abrahams, G. E. Hawkes, J. Mater. Sci.: Mater. Med. **19**, 1687 (2008).
[8] A. Lin, N. S. Mcintyre, R. D. Davidson, J. Dent. Res. **71**, 1836 (1992).
[9] Q. Zeng, F. Stebbins, Am. Mineral. **85**, 863 (2000).
[10] C. K. Y. Yiu, F. R. Tay, N. M. King, D. H. Pashley, S. K. Sidhu, J. C. L. Neo, M. Toledano, S. L. Wong, J. Dent. Res., **83**, 283 (2004).
[11] Y. Yoshida, K. Shirai, Y. Nakayama, M. Itoh, M. Okazaki, H. Shintani, S. Inoue, P. Lambrechts, G. Vanherle, B. Van Meerbeek, J. Dent. Res., **81**, 270 (2002).
[12] A. Karmaker, A. Prasad, N. K. Sarkar, J. Mater. Sci.: Mater. Med. **18**, 1157 (2007).
[13] T. Kokubo, H. M. Kim, M. Kawashita, Biomaterials, **24**, 2161 (2003).
[14] D. Massiot, F. Fayon, M. Capron, I. King, S. Le Calve, B. Alonso, J.-O. Durand, B. Bujoli, Z. Gan, G. Hoatson, Magn. Res. Chem., **40**, 70 (2002).
[15] R. H. Halvorson, R. L. Erickson, C. L. Davidson, Dent. Mater. **19**, 327 (2003).
[16] N. Zotov, H. Keppler, Am. Mineral. **83**, 823 (1998).
[17] B. N. Roy, J. Am. Ceram. Soc. **73**, 846 (1990).
[18] J. P. Hamilton, S. L. Brantley, C. G. Pantano, L. J. Criscenti, J. D. Kubicki, Geochim. Cosmochim. Acta, **65**, 3683 (2001).
[19] S. Abiraman, H. K. Varma, T. V. Kumari, P. R. Umashankar, A. John, Bull. Mater. Sci. **25**, 419 (2002).
[20] K. N. Dalby, P. L. King, Am. Mineral. **91**, 1783 (2006).
[21] A. Madani, A. Aznar, J. Sanza, J. M. Serratosa, J. Phys. Chem. **94**, 760 (1990).
[22] B. T. Poe, P. F. McMillan, C. A. Angell, R. K. Sato, Chem. Geology **96**, 333 (1992).
[23] H. Scholze, Glass: Nature, Structure and Properties. New York: Springer; 1991, p. 137.
[24] M. H. Bhat, M. Ganguli, K. J. Rao, Curr. Sci. India, **86**, 676 (2004).
[25] E. I. Kamitsos, M. A. Karakassides, G.D. Chryssikos, J. Phys. Chem., **91**, 5807 (1987).
[26] L. Baia, S. Simon, W. Kiefer, Phys. Chem. Glasses, **46**, 279 (2005).
[27] D. Peak, G.W. Luther III, D.L. Sparks, Geochim. Cosmochim. Acta, **67**, 2551 (2003).
[28] J. Torrent-Burgues, R. Rodriguez-Clemente, Cryst. Res. Technol., **36,** 1075 (2001).
[29] S. Matsuya, T. Maeda, M. Ohta, J. Dent. Res., **75**,1920 (1996).
[30] P. Zhang, P. J. Grandinetti, J. F. Stebbins, J. Phys. Chem. B, **101**, 4004 (1997).
[31] E. F. S. Vieira, J. D. A. Simoni, C. Airoldi, J. Mater. Chem., **7**, 2249 (1997).
[32] S. Prasad, T. M. Clark, T. H. Sefzik, H.-T. Kwak, Z. Gan, P. J .Grandinetti, J. Non-Cryst. Solids, **352**, 2834 (2006).
[33] J. A. Kerr, in CRC Handbook of Chemistry and Physics, ed. J.A. Lide, Boca Raton, Florida, CRC Press; 2000.
[34] S. K. Lee, J. F. Stebbins, **84**, 937 (1999).
[35] G. Engelhardt, M. Noftz, K. Forkel, F. G. Wishmann, M. Magi, A. Samson, E. Lippma, Phys. Chem. Glasses, **26**, 157 (1985).
[36] M. E. Smith, Solid State Nucl. Magn. Res., **3**, 111 (1994).
[37] R. K. Sato, P. F. McMillan, P. Dennison, R. Dupree, J. Phys. Chem., **95**, 4483 (1991).
[38] D. Iuga, S. Simon, A. P. M. Kentgens, E. De Boer, J. Phys. Chem B, **3**, 7591 (1999).
[39] P. E. Stallworth, P. J. Bray, in Glass Science and Technology, eds. D.R. Uhlmann, N.J. Kreidl, Boston, Acad Press Inc, 1990. p. 77-100.

[40] B. C. Bunker, R. J. Kirkpatrick, R. K. Brow, G. L. Turner, C. Nelson, J. Am. Ceram. Soc. **74**, 1430 (1991).
[41] R. K. Brow, D. R. Tallant, G. L. Turner, J. Am. Ceram. Soc., **79**, 2410 (1996).
[42] S. Simon, G. J. M. P. Van Moorsel, A. P. M. Kentgens, E. De Boer, Solid State Nucl. Mag., **5**, 163 (1995).
[43] L. Züchner, J. C. C. Chan, W. Müller-Warmuth, H. Eckert, J. Phys. Chem. B, **102**, 4495 (1998).
[44] J. F. Stebbins, S. Kroeker, S. K. Lee, T. J. Kiczenski, J. Non-Cryst. Solids, **275**, 1 (2000).
[45] S. Sen, Z. Xu, J. F. Stebbins, J. Non-Cryst. Solids, **226**, 29 (1998).
[46] N. Tsomaia, S. L. Brantley, J. P. Hamilton, C. G. Pantano, K. T. Mueller, Am. Mineral., **88**, 54 (2003).
[47] V. Sundaramurthy, I. Eswaramoorthi, N. Lingappan, Can. J. Chem., **82**, 631 (2004).
[48] M. Środa, Z.Olejniczak, Opt. Appl., **38**, 259 (2008).
[49] S. Kroeker, J. F. Stebbins, Inorg. Chem., **40**, 6239 (2001).
[50] W. F. Mousa, M. Kobayashi, Y. Kitamura, I. A. Zeineldin, T. Nakamura, J. Biomed. Mater. Res., **47**, 336 (1999).
[51] Q. Z. Chen, K. Rezwan, D. Armitage, S. N. Nazhat, A. R. Boccaccini, J. Mater. Sci.: Mater. Med., **17**, 979 (2006).

*Corresponding author: simons@phys.ubbcluj.ro